ISPRS Int. J. Geo-Inf. **2013**, *2*, 797-816; doi:10.3390/ijgi2030797

OPEN ACCESS
ISPRS International Journal of **Geo-Information**
ISSN 2220-9964
www.mdpi.com/journal/ijgi/

Article

A Comparison of Precise Leveling and Persistent Scatterer SAR Interferometry for Building Subsidence Rate Measurement

Kirsi Karila *, Mika Karjalainen, Juha Hyyppä, Jarkko Koskinen, Veikko Saaranen and Paavo Rouhiainen

Finnish Geodetic Institute, Geodeetinrinne 2, FI-02431 Masala, Finland;
E-Mails: mika.karjalainen@fgi.fi (M.K.); juha.hyyppa@fgi.fi (J.H.); jarkko.koskinen@fgi.fi (J.K.); veikko.saaranen@fgi.fi (V.K.); paavo.rouhiainen@fgi.fi (P.R.)

***** Author to whom correspondence should be addressed; E-Mail: Kirsi.Karila@fgi.fi; Tel.: +358-9-295-550; Fax: +358-9-295-55-211.

Received: 20 June 2013; in revised form: 1 August 2013 / Accepted: 15 August 2013 / Published: 21 August 2013

Abstract: It is well known that the most accurate method to detect changes of height is the geodetic precise leveling method. Due to the high demand work and time needed for precise leveling alternative methods are studied to obtain high quality height information. Differential SAR interferometry techniques such as the Persistent Scatterer Interferometry (PSI) method are studied to detect millimeter level deformations in urban areas. Additionally, SAR analysis will provide spatially extensive information on subsidence. On the other hand, PSI subsidence rates have not yet been comprehensively compared to the precise leveling measurements of the subsidence of individual buildings. Typically subsidence rates are interpolated to a continuous spatial surface, but in this study, spatially discontinuous subsidence was measured for a set of individual buildings. Therefore, we conducted three precise leveling campaigns and measured in total 82 geodetic-grade bolts, which were tightly attached to the building foundations. Moreover, we used additional leveling data (obtained from the local authorities), which contained long time series of leveling data for individual buildings. In the present study, ERS and ENVISAT satellite SAR data were processed using a PSI algorithm and the results were compared to leveling data of individual buildings.

Keywords: persistent scatterer interferometry PSI; precise leveling; discontinuous urban subsidence; SAR; Turku

1. Introduction

Synthetic Aperture Radar (SAR) interferometry has been widely used for detecting surface deformations in numerous areas worldwide. Leveling is the traditional ground surveying method to measure height and height changes. Furthermore, the precise leveling method is a more sophisticated leveling procedure and very accurate height measurements can be carried out [1]. However, to cover an area of a several km^2 with leveling measurements is time-consuming and expensive. It is well known, that satellite-borne SAR images offer a good spatial coverage and in favorable conditions even millimeter-level deformation rates can be detected in urban areas, e.g., [1,2]. The objective of the present study was to apply a persistent scatterer interferometry (PSI) technique to detect the spatially discontinuous building subsidence in the city of Turku and compare the results to precise leveling data of individual building foundations.

Persistent scatterer interferometry (PSI) was developed [3] to improve the applicability of differential SAR interferometry (DINSAR) [4]. The PSI techniques offer a high precision in deformation measurements, even down to the sub-millimeter level [2]. Several algorithms exist for deformation detection using PSI, e.g., [5–9]. Combination of ERS and ENVISAT time series in PSI has been presented in, e.g., [10–13].

The validation of DINSAR and PSI results can be carried out using different methodologies. First, a DINSAR cross-comparison (e.g., in [14,15]) can be carried out when the same dataset is processed using different DINSAR or PSI algorithms, or using the same algorithm to process an independent SAR dataset, for instance ascending and descending datasets or data from a different SAR sensors. Second, to study the absolute accuracy, ground truth data are required. Precise ground measurements can be carried out using traditional surveying methods, such as leveling and the global navigation satellite system (GNSS) or borehole extensometers. Precision comparable to PSI is only possible using repeated precise leveling campaigns or a very long time series based on permanent GNSS stations, and with special equipment and algorithms. The surveying profiles can be compared against SAR subsidence maps as in [14,16–18], and artificial corner reflectors can be used for the DINSAR phase calibration [19–21]. Many studies have been carried out dealing with the validation of continuous subsidence phenomena measured using PSI, e.g., [14,16,22]. Previous works regarding the PSI monitoring of urban structures and infrastructures include [23–27].

The most precise measurements of elevation changes are obtained by leveling measurements. However, the accuracy of leveling depends on the equipment and methods used. The most accurate results are obtained using a precise leveling instrument and procedure [1,28]. For example, according to [29], the standard kilometer error for the precise leveling results was less than 1 $mm/(km^{1/2})$.

Building subsidence measurements are based on monitoring the position of metal bolts located in the stone foundations of the buildings. Since leveling is a relational measurement method the surveys

have to be tied to a stable point, usually a benchmark bolt in bedrock, which can be considered stable for longer periods of time.

A brief comparison of the precise leveling and PSI techniques is presented in Table 1. For measuring subsidence in city areas PSI can provide better spatial point density than ground survey measurements. According to [30], the average PS density in urban areas is between 0.5% and 2.5% of the original number of pixels, corresponding to 50–400 points per km^2, which is much higher than the densities obtained using ground survey methods. Perissin and Rocca [31] have demonstrated that the positioning accuracy of a PS is within 1 m in all three directions if a large number of SAR scenes are used. However, in the basic PSI algorithms the PS location is not determined with such precision. The major advantage of the DINSAR techniques over the leveling measurements would be their more extensive spatial coverage, cost and more frequent monitoring. More comprehensive discussion and PS density for different SAR sensors, the frequency, and the cost compared with in-situ techniques is studied for different types of deformation is available in [32].

Table 1. A short comparison of precise leveling and persistent scatterer interferometry (PSI) techniques.

	Precise Leveling	**PSI**
Temporal aspects	Roughly 20–50 benchmarks/day, campaign repeated several times	Data available every 11–46 days (+archived data), processing takes only a few hours or days
Human resources	3–4 (survey), 1 post processing	1
Other resources	Instruments, benchmarks, travelling costs, leveling software	Time series of satellite data (20-), PSI software
Observation density	Lines, Tens/km^2 (targets can be selected)	Hundreds/km^2 (built-up area, where PS are available)
Displacement detected	Height	Radar line-of-sight
Accuracy	Sub-millimeter	mm

2. Site and Data

2.1. Site

The city of Turku, on the southwest coast of Finland (Figure 1), was founded in the 13th century and is the former capital of Finland. It is located at the mouth of the River Aurajoki and clay and bedrock areas alternate in the area (Figure 2). A part of the city has been built on a clay layer of tens of meters thick. The clay soil of the river valley is the reason for the severe subsidence problems the city is facing today. A geological description of the area is available in [33].

Turku was selected as the study area because severe building subsidence has been reported there [34]. In Turku, some of the buildings in clay areas are subsiding with respect to the ground. Several buildings still rest on wooden pilings, and as the ground water level drops in these clay areas the old wooden pilings decompose, resulting in building subsidence and structural damage. Renovation

works are continuously ongoing in the city. In 2003, the cost of renewing all the damaged pilings was estimated to be around 100–200 million Euros [35].

Figure 1. Location of Turku. Map data (c) OpenStreetMap.org contributors, CC-BY-SA.

Figure 2. An example cross-section of the soil types in the area. Modified from [33].

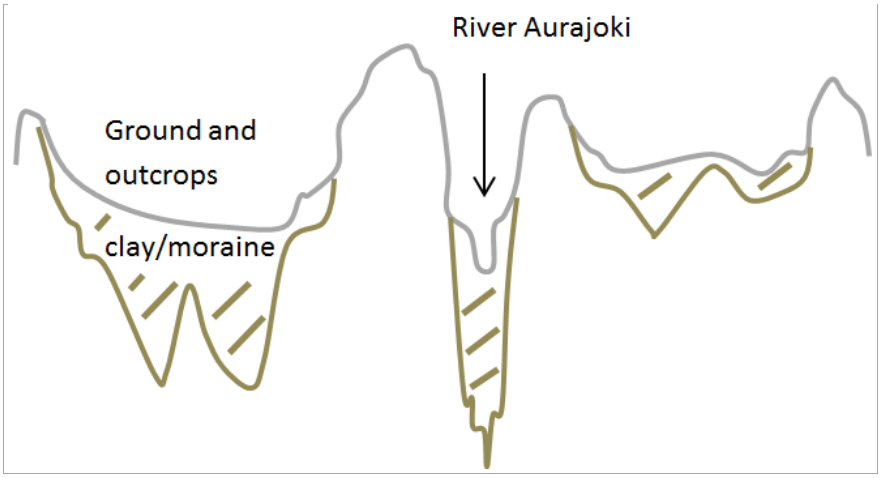

The city is surrounded by agricultural land, forests, and the sea. The central part of the city is more densely built up; covering an area of several square kilometers, and the entire city includes a great deal of vegetation cover. Due to the marked seasonal variation in vegetation and temporal coherence, the traditional DINSAR is not feasible, and therefore, a PSI technique needs to be applied.

The subsidence in Turku was studied using ERS data in [23], and in the present study, ENVISAT ASAR data and the results of three precise leveling campaigns were added. Before that work, DINSAR techniques have not been applied to the study of ground deformations or urban subsidence in Finland, probably due to the significant vegetation coverage in urban area and small urban areas. Due to the stable bedrock, unexpected movements are not common in Finland. However, in Turku, building

subsidence is occurring in clay soil areas and causing damage to buildings. For many years, the building subsidence has been monitored by leveling measurements, and the results indicate constant annual subsidence rates from 0 mm/yr to 7 mm/yr. Therefore, Turku is a good test site for PSI, since subsidence exhibits a linear behavior. This is discussed further in the ends of Section 4.1.

2.2. SAR Data

A set of ERS-1, ERS-2, and ENVISAT single look complex (SLC) SAR images was acquired for the study area. The satellite images cover the period from 1992 to 2005. A total of 34 ERS scenes and eight ENVISAT (Table 2) scenes were selected for use in this study. ERS and ENVISAT images have the same imaging geometry (look angle, track, descending acquisition), thus the same persistent scatterers are detectable in the images. Pixel spacing of the images is 4 m in azimuth and 20 m in ground range.

Table 2. SAR data (ERS and ENVISAT, Track 494, Frame 2388), date and the perpendicular beseline. The master images are in italics.

Satellite	Date	Baseline$_\perp$	Satellite	Date	Baseline$_\perp$	Satellite	Date	Baseline$_\perp$	Satellite	Date	Baseline$_\perp$
ERS1	01.05.92	−880	ERS1	18.02.96	402	ERS2	08.06.98	673	ERS2	30.09.02	474
ERS1	05.06.92	−159	ERS2	19.02.96	541	ERS2	13.07.98	−613	ENVISAT	04.11.02	−320
ERS1	01.01.93	−771	ERS1	28.04.96	417	ERS2	17.08.98	−355	ENVISAT	24.03.03	−163
ERS1	05.02.93	−598	ERS2	29.04.96	335	ERS2	19.04.99	305	ENVISAT	28.04.03	930
ERS1	16.04.93	846	ERS1	02.06.96	−348	ERS2	24.05.99	161	ENVISAT	15.09.03	140
ERS1	25.06.93	−363	ERS2	03.06.96	−377	ERS2	28.06.99	284	ENVISAT	02.02.04	609
ERS1	30.07.93	−127	ERS2	16.09.96	−146	ERS2	02.08.99	284	*ENVISAT*	*15.08.05*	*0*
ERS1	03.09.93	−22	ERS2	01.09.97	369	ERS2	06.09.99	−659	ENVISAT	31.07.06	486
ERS2	19.06.95	−351	ERS2	06.10.97	154	ERS2	08.04.02	−179	ENVISAT	04.09.06	347
ERS1	*27.08.95*	*0*	ERS2	30.03.98	−20	ERS2	13.05.02	−603			
ERS2	28.08.95	−14	ERS2	04.05.98	444	ERS2	17.06.02	440			

2.3. Leveling and Auxiliary Data

The leveling data is described in more detail in Section 3.2. Aerial images, a city base map, and a digital elevation model (25 m × 25 m grid size) were used as auxiliary data.

3. Methods

3.1. PSI Processing

In PSI processing, the Coherent Target Monitoring (CTM) algorithm [9,36,37] that makes use of long-term stable pixels (PSs), called coherent targets, was used. The coherent targets are selected on the basis of the temporal coherence (TC) of a pixel. The temporal coherence is a measure describing how stable the phase of a scatterer is over time. CTM algorithm uses information from distributed targets as well as point like target.

The phase of a differential interferogram where the topographic phase and the flat earth phase terms have been removed is

$$\phi_{diff} = \phi_{defo} + \phi_{atmo} + \phi_{dem\_error} + \phi_{noise} \quad (1)$$

where the phase components are deformation, atmospheric delay, residual topographic phase (DEM error) and noise. A stable reference area is chosen for the initial atmospheric phase estimate. Initially, the atmosphere is expected to be constant over the processing region. By subtracting the average phase of the reference area we get the atmosphere corrected interferogram

$$\phi_{aci} = \phi_{defo} + \phi_{dem\_error} + \phi_{noise} \quad (2)$$

Phase corresponding to a DEM error value and slope of a linear deformation model are used to calculate the residual phase

$$\phi_i = \phi_{aci} - \phi_{defo} - \phi_{dem\_eror} \quad (3)$$

The DEM error and slope are determined using the temporal coherence of a pixel

$$\gamma = \frac{\sqrt{\left(\sum_i \cos(\phi_i)\right)^2 + \left(\sum_i \sin(\phi_i)\right)^2}}{n} \quad (4)$$

where i(1, …, n) is the interferogram and n is the total number of interferograms. The DEM error and slope pair that gives the highest temporal coherence is searched (template search, user-defined range). As a result, estimates for DEM error, deformation rate and TC are obtained.

In subsequent iterations, the atmospheric estimate is refined by subtracting the estimates of ϕ_{defo} and ϕ_{dem_error} from the differential phase and smoothing it over the area to get a new estimate for the ϕ_{atmo}. For this, only pixels having a TC above a user-defined threshold are used. The new estimate of ϕ_{atmo} is then subtracted from the original differential phase to obtain a new atmosphere corrected interferogram, which is used in the search for new slope and DEM error values, and subsequently, new temporal coherence estimates are obtained.

In our study, the time series of the ERS and ENVISAT images were formed separately; hence cross-interferograms were not formed. The ERS and ENVISAT master images were co-registered. Thus, all of the ERS and ENVISAT images had a common reference grid, and thus, several common PSs can be found both in ERS and ENVISAT time series. A common region-of-interest (ROI) of 6 km × 15 km was chosen for interferometric processing. A simulated interferogram was obtained from the DEM and co-registered to the master image, in order to get the topographic phase of the interferograms.

First, the ERS time series of 33 interferograms was formed. The ERS master image (27.8.95) was selected to have a reasonable dispersion of geometrical and temporal baselines. The image processing steps are image co-registration to common master image, selection of region of interest, and the computation of differential interferograms using the topographic phase from the DEM and Delft (DEOS) precise orbits.

Secondly, the ENVISAT time series of seven interferograms was formed similarly. The ENVISAT master was selected to represent the same time of year as the ERS master, in order avoid effects due to seasonal variation in ERS master and ENVISAT master image co-registration.

A ROI (4.7 km × 4.4 km) for the PSI processing was selected from the differential interferogram stack. A known non-subsiding area in the center of the city was selected as the reference for zero

deformation and for the estimation of the initial atmospheric offset. Deformation rates are estimated relative to this reference area. The area is presented in Figure 3.

Figure 3. Real Estate Department of Turku (REDT) and Finnish Geodetic Institute(FGI) leveling benchmarks and their vertical deformation rates in the area. Yellow is stable point. Red square marks the approximate position of the initial atmosphere estimate. Numbers mark the buildings measured by REDT. Aerial image © Turun kaupungin Kiinteistöliikelaitos.

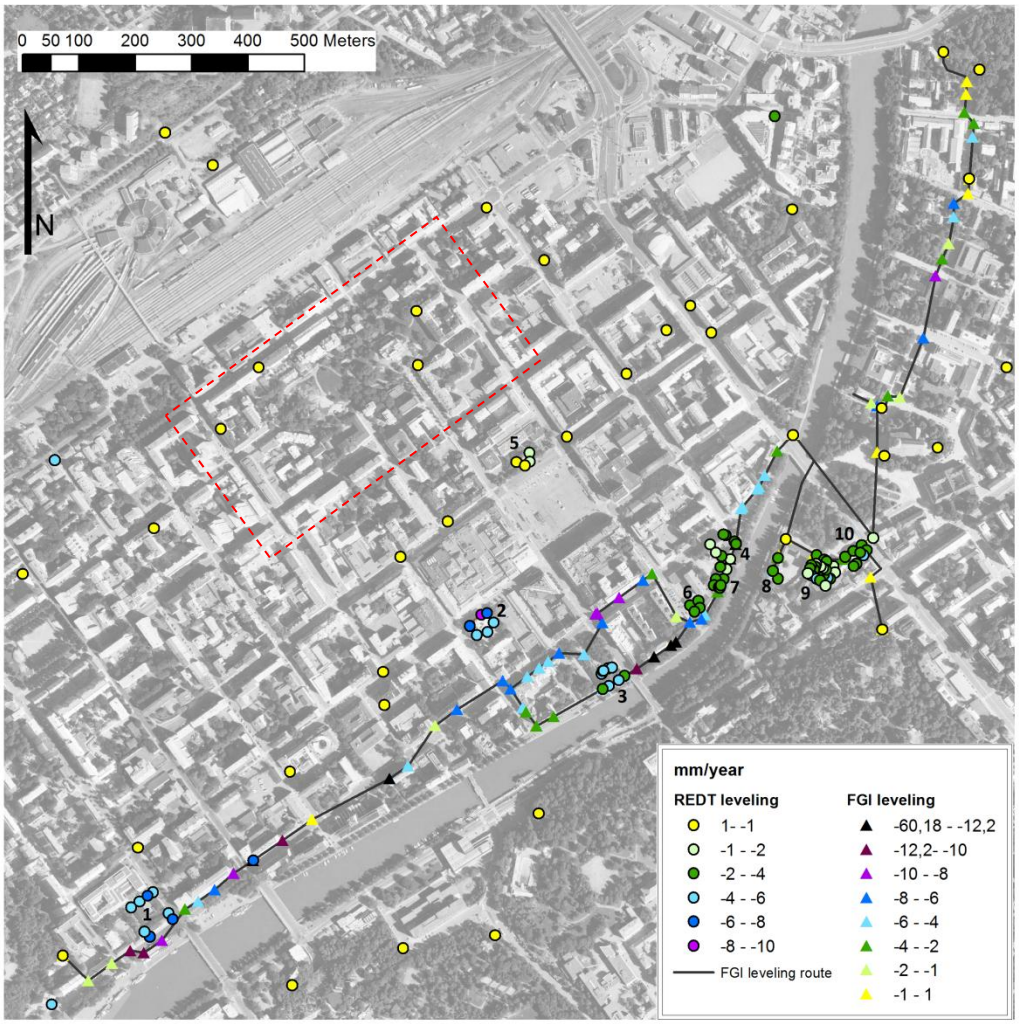

Then, the iterative process was executed to separate the phase terms due to deformation, atmosphere change and DEM error. In the template search, maximum deformation slope was set ±0.5 cycle/yr, and 0.025 cycles/yr (~0.7 mm/yr) increments were used, for DEM error maximum of ±20 m and increments of 1 m were used. The temporal coherence estimate is refined during each iteration round and new PSs are found. The TC threshold for atmospheric refinement was 0.65, and for the output products (deformation maps) the TC thresholds of 0.6, 0.65 and 0.7 were used. In the atmospheric refinement, the atmospheric screen smoothing length was 2,000 m. A linear model was used for the deformation. The slope of the deformation model is estimated using both the ERS and ENVISAT time series and both time series are fitted to the model. Therefore, the final deformation estimation is done using information from the both time series. Finally, the line-of-sight deformation is converted to vertical deformation. Two iteration rounds were performed. Adding more iteration rounds did not

make a significant difference to the annual subsidence rates. The second iteration results were used in the following analyses.

In addition to determining the deformation rate, the PSI processing also provides an estimate of the digital elevation model (DEM) error and temporal coherence of the PS. The DEM error is the difference between the reference DEM height and the height of the scatterer, e.g., the scatterer may be on top of a building.

3.2. Establishing a Validation Network for Subsidence Monitoring Based on Precise Leveling

Two different sets of leveling data were used as a reference in this study, one set from Turku City's Real Estate Department (REDT) and one set was measured by FGI.

The subsidence of buildings in Turku has been monitored for decades on the basis of leveling measurements carried out by the city authorities and private companies. This includes a leveling dataset held by the City's Real Estate Department (REDT) covering a number of City-owned buildings in the downtown area. The REDT leveling data contains several observations for each building, e.g., in all corners of the buildings and in the middle. The data were acquired between 1990 and 2003, though the coverage varies from one building to another, and contains data on several bolts for each building. The monitored buildings were those where damage had been observed. Ten buildings (including 76 benchmarks) were monitored in the city center area. In addition, tens of height control points are monitored in the area. The measurements were done separately for each building. The accuracy of these measurements is not known. The results have been documented with 1 mm precision. Taking into account the accuracy of standard leveling devices, the accuracy should within a few millimeters. Based on the REDT leveling data, linear subsidence rates can be assumed in the test area. Differential settlement is likely in building "Koulu" (2.9 mm/yr) and "Cathedral school" (1.8 mm/yr). For the other buildings, it is about 1 mm/yr or less, which can be caused by the measurement error. The REDT leveling benchmarks and rates are shown in Figure 3.

In order to validate the PSI results more comprehensively, FGI established a PSI test site in the center of Turku in 2005. Precise leveling was chosen as the measurement method, since it is still the most accurate method available.

Figure 4. An example of a levelling benchmark (photo: Veikko Saaranen).

A large number of buildings already had metal bolts (Figure 4) mounted on their stone foundations as a result of the known subsidence problems in the area. All bolts were already installed on buildings by the city authorities or private companies, which have been monitoring the buildings. Fourteen of these bolts were also used in the REDT measurements. The measurements were tied to three bolts in the bedrock (Table 3), and these were considered to remain stable. The digital leveling system Zeiss DiNi12 with LD12 and LD13 bar code invar rods were used in the measurements.

Table 3. Bedrock benchmark list.

	X (ETRS-GK23)	Y (ETRS-GK23)	Z (N2000)
4545	6,705,385.2	23,460,366.6	13.793
3030	67,04,371.8	23,460,232.6	15.207
3639	6,703,842.6	23,458,753.6	10.414

The FGI precise leveling route is about 4.9 km long and covers the main subsidence area along the river. It is comprised of 82 bolts on the outside of buildings and the three bedrock benchmarks. The bolts are made of metal and mounted on the stone foundations of the buildings. Redundancy was considered in the leveling network design, and a number of loops were measured. The resulting leveling network is basically a leveling line through the city with two loops in the middle. This allowed more reliable results to be obtained and certain buildings of special interest to be included. Extending the test site to encompass other major subsidence locations, such as the area around the railway station, would be relatively straightforward, as these other locations also include bolts mounted in bedrock and on building foundations. However, it was not done due to the time required to complete the measurements.

The FGI has three sets of precise leveling measurements, the first from May 2005, the second from October 2005, and the third from June 2006. The network adjustment was carried out using program "Local X-positioning system" [38]. The adjustment method was a constrained net with the three bedrock benchmarks fixed. The weight of each observation was inversely proportional to the distance of the benchmark interval. A posteriori standard deviations for the campaigns were 0.65 mm/($km^{1/2}$), 1.05 mm/($km^{1/2}$), 0.94 mm/($km^{1/2}$). The results are stored as a set of point data containing the three observations for each point and the annual subsidence rate derived from these measurements. Average subsidence was 4.7 mm/yr and standard deviation was 3.6 mm/yr. Maximum measured displacement was 60 mm/yr (in a building being renovated at the time) and minimum was zero. FGI's leveling test site is presented in Figure 3 and described in more detail in [39].

3.3. Comparison

When a deformation phenomenon is spatially continuous, the deformation can be modeled, and, point-wise PS observations have to be interpolated to obtain a continuous deformation field. Geostatistical methods, such as kriging in [40], are often used for interpolation. However, when the deformation is spatially non-continuous (adjacent buildings can be stable or subsiding depending on the condition of the foundations), as in the Turku case, the situation is less straightforward, requiring the corresponding PSI observations and ground survey benchmarks to be determined. Since the density of PS is usually higher than the density of benchmarks, the alternatives are either to use the closest PS

or every PS within a certain distance from the benchmark. The geocoding of each PS is rough, *i.e.*, the closest PS in not necessarily the closest in reality, and also there are several PSs in one building. In the following analyses, the closest PS that was inside the building borders was used. (Figure 5) Maximum distance of 20 m was applied.

Figure 5. 11 PS, eight REDT and two FGI leveling benchmarks and their vertical deformation rates in Town Hall. Selection of the closest PS for two FGI benchmarks is shown with arrows. For mean annual PSI rate all 11 PS were used.

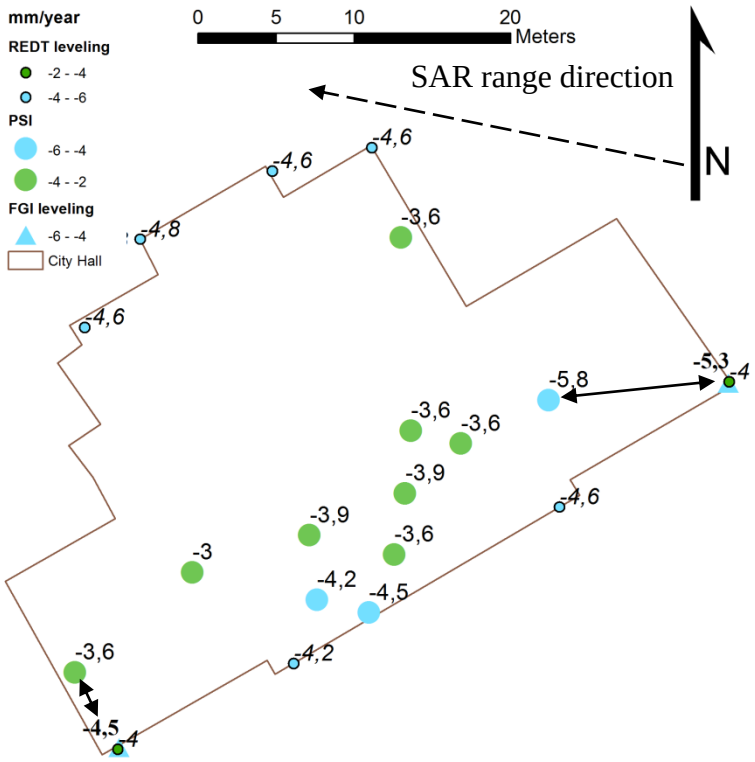

The geocoding of PSI results is not easy because of the different reference systems of the SAR data and the city maps. In addition, the scatterer is not necessarily situated in the center of the resolution element but is instead only known to be within the area of a resolution element. As a result of a PSI analysis, the height of the scatterer or the error of its height with respect to the DEM, used can be further used during the geocoding. However, an incorrect height estimate will lead to false geocoding. Fortunately, the PS observations are usually clustered, and this helps to relate the geocoded PS observations to ground objects, such as buildings. The geocoding accuracy of the PS with respect to the map data was visually estimated by comparing PSs to the building map. The maximum geocoding error was estimated to be circa 5 m in azimuth (~North-South direction) and circa 20 m in ground range direction (~East-West). This is similar to the ERS SLC image nominal resolution, which is 10 m in slant range and 5 m in azimuth direction.

In the Turku case study, the building data of Turku city digital base map were used to study the spatial distribution of the persistent scatterers. By using this data, it was possible to determine corresponding coherent targets and buildings. A set of aerial images was used for visual inspection purposes.

The REDT leveling data subsidence rates for a certain building part were very similar, thus, the leveling observations could be converted to mean annual subsidence velocity of the building or a part

of a large building. It is also more convenient to relate the geocoded PSs to larger objects, e.g., a part of a building. The building data of the digital city base map was used in identifying the corresponding radar scatterers of certain buildings. The REDT observations were digitized on the base map. An overlay analysis of the leveling and SAR datasets was carried out. In order to compare the REDT leveling results and the PSI results, the mean annual deformation rates were calculated for different buildings or building parts. For the mean annual rates, all of the PS within building borders (or less than 2 m from border) were used.

4. Results

The results of the PSI analysis of the SAR data were studied, and the deformation rates were classified as follows: stable (−2–+2 mm/yr), uplift (>2 mm/yr), and subsidence (<−2 mm/yr). Different TC threshold values were used. The results are listed in Table 4. When a higher TC threshold value is applied the number of PSs indicating subsidence and uplift decreases. In order to obtain reliable results, the threshold value applied should be as high as possible, although enough PS should remain. The PSI result is presented in Figure 6.

Table 4. A classification of the PSI observations using different Temporal Coherence (TC) thresholds.

TC Threshold	# PS	Stable	Subsidence	Uplift
TC > 0.6	16,138	79%	19%	2%
TC > 0.65	8,805	84%	16%	0.02%
TC > 0.7	4,384	86%	14%	0.0007%

Figure 6. The PSI subsidence map of Turku. The vertical deformation rates are in mm/yr. The black line is the FGI leveling network, which includes three bedrock bolts (the black triangles). TC ≥ 0.6. The coordinates are in the Finnish National Coordinate System (KKJ). Aerial image © Turun kaupungin Kiinteistöliikelaitos.

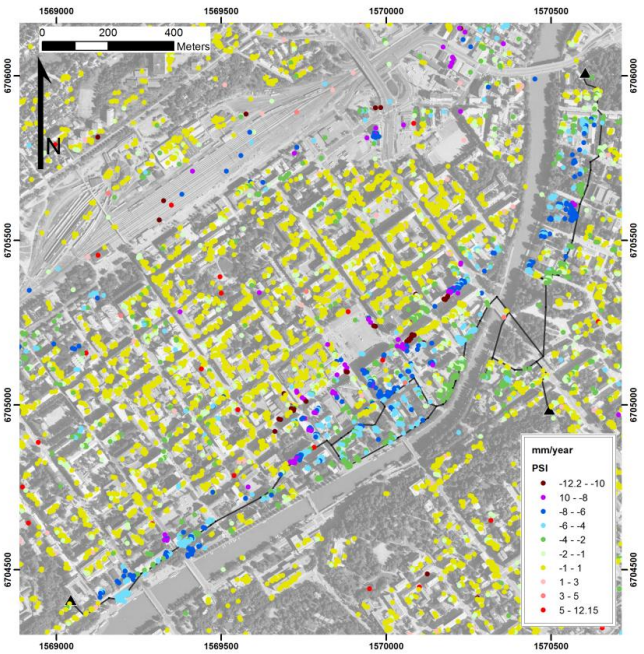

4.1. Comparison with the REDT Leveling Data

For 10 buildings the annual mean subsidence rates from the REDT leveling data (mean of the benchmarks in the building foundations) and PSI (mean of the PS located on the building) were compared. The results are shown in Table 5. The mean subsidence rates are similar; however, single observations vary as seen from the maximum and minimum observations. R^2 value of the mean deformation rates is 0.96 and the mean deformation rate from PSI is on average 0.03 mm/yr slower than the mean rate from leveling.

Table 5. The vertical motion rates per year for 10 different buildings from the PSI processing and the REDT leveling measurements. Mean deformation rate from PSI is on average 0.03 mm/yr slower than the mean rate from leveling. The locations of the buildings can be found in Figure 3.

Building	PSI mean Deformation	PSI Maximum Deform. Rate	PSI Minimum Deform. rate	Number of PS	Mean Deformation Rate from Leveling	Maximum Deform. Rate from Leveling	Minimum Deform. Rate from Leveling	Leveling Bench-Marks	REDT-PSI
1. Linnakatu 39	**−6.1**	−7.9	−4.6	13	**−5.8**	−6.6	−5.1	8	0.3
2. Koulu Brewery	**−7.2**	−9.4	−5.5	7	**−6.6**	−8.1	−5.2	6	0.6
3. Town Hall	**−3.9**	−5.8	−3.0	11	**−4.4**	−4.8	−4.0	8	−0.5
4. Library	**−2.0**	−4.5	−1.2	18	**−2.2**	−2.6	−1.4	9	−0.2
5. Orth. church	**−0.1**	−0.6	0	7	**−1**	−1.5	−0.3	4	−0.9
6. Art Hall	**−3.9**	−3.9	−3.6	4	**−4**	−4	−4	4	−0.1
7. Music Library	**−3.0**	−3.9	−2.1	9	**−2.8**	−3.7	−1.8	8	0.2
8.Cathedral school	**−3.7**	−4.2	−3.3	6	**−3.3**	−4	−2.2	3	0.4
9. Hjelt house	**−3.0**	−3.0	−3.0	1	**−3.5**	−5	−3	8	−0.5
10. Brinkkala house	**−3.2**	−4.8	−2.1	9	**−2.8**	−5	−2	18	0.4

Table 6. Absolute difference of the single PS observations to the linear model based on REDT leveling observations in Figure 7. In addition, the difference of single ERS PSs and ENVISAT PSs to linear model based on the PSI data is presented.

	Average Absolute Value of the Difference to Leveling	Maximum Absolute Value of the Difference to Leveling	Minimum Absolute Value of the Difference to Leveling	Average Absolute Difference ERS-PSs To PSI Linear Model	Average Absolute Difference of Envisat-PSs to PSI Linear Model
Koulu PS1	**4,1**	14,4	0,2	3,5	5,5
Koulu PS2	**11,8**	28,7	1,7	3,4	3,1
Town Hall PS1	**4,0**	12,7	0,0	2,8	3,2
Town Hall PS2	**8,6**	23,7	1,2	3,4	3,9
Linnakatu39 PS1	**3,4**	11,5	0,1	3,1	3,7
Linnakatu39 PS2	**14,4**	32,1	3,1	3,0	4,7

Six PSI time series are plotted against three REDT leveling time series in Figure 7. Single observations have remarkable phase noise and are unreliable, however, on average, good results can be obtained. The average deformation rates vary from PS to PS, and only few match perfectly with the leveling time series. PS deformation rates differences to linear model based on leveling data are presented in Table 6. Even though, the ENVISAT time series is short and thus, lower accuracy can be

expected as a result of higher deviation of deformation values (average difference from linear PSI model is 3.2 for ERS and 4.0 for Envisat, Table 6), the observations can be combined with the ERS time series.

Figure 7. The ERS and ENVISAT time series for 2 PS on three buildings and the linear subsidence based on the PSI observations. For comparison, a REDT leveling time series for a benchmark located in the building is presented. Deformation is zero for the ERS master image.

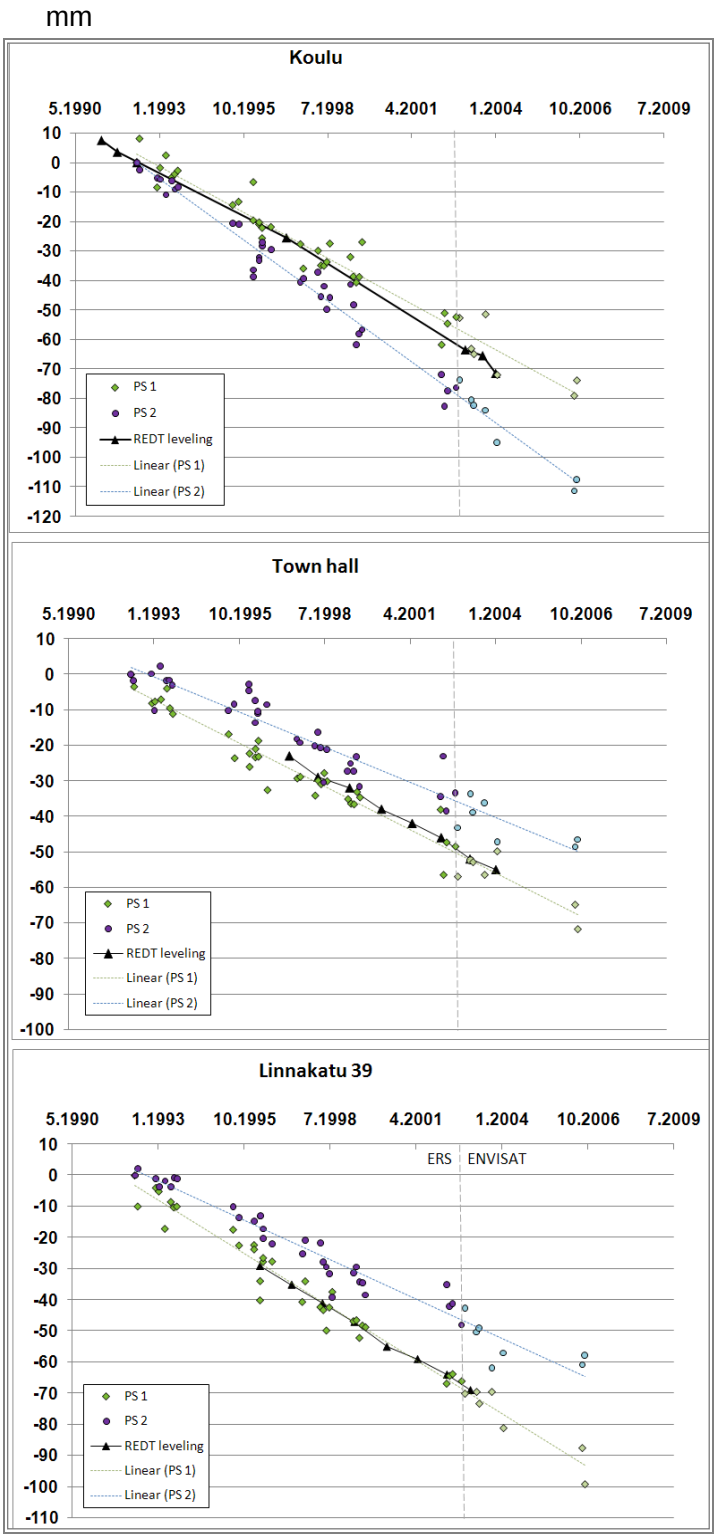

Some possible causes for the single observation deviation in Figure 7 are presented here. For the last four ERS (ERS-2 satellite) observations from 2002, differences are large between images from the Doppler centroid and the master image, which causes decorrelation between images. In the SAR images acquired 18.2.1996 and 19.2.1996, there is ca. 30 cm snow, which may cover some of the PS, e.g., the Linnakatu 39 target shows significant deviations in Figure 7. Geometrical decorrelation due to long baselines (over 700 m in Table 2) may lower the accuracy of these estimates. Geometrical decorrelation and reaction to snow cover depends on the structure of the PS, therefore the effect is remarkable only in some of the PS.

We also noticed that in Figure 7 the leveling observations for all three benchmarks fit the line with an R^2 value of higher than 0.99. This supports the assumption of linear subsidence in Turku.

4.2. Comparison with the FGI Leveling Data

For the comparison with FGI leveling data, all the subsidence rates were converted to the mean annual subsidence rates. The PSs geocoding was refined using aerial images. An overlay operation was carried out in order to determine the PS of each part of the buildings corresponding to the leveling benchmark. In comparing the PS observations with the leveling observations, a maximum distance of 20 m from the leveling observation was set. This distance was considered appropriate in view of the geocoding accuracy for the PSs and the SAR resolution.

Figure 8. The PS subsidence compared to the FGI precise leveling results.

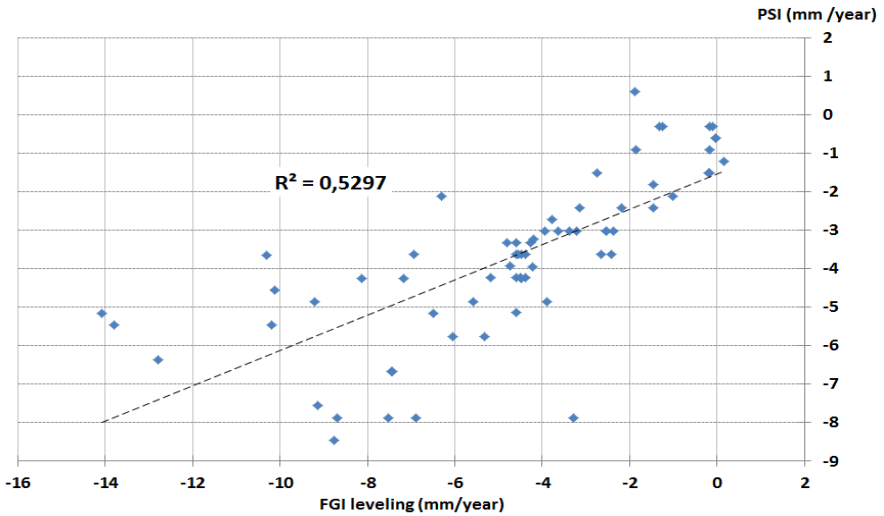

For 65 of the leveling benchmarks a nearby PSI observation was available. The annual subsidence rates were compared (Figure 8). The R^2 value was 0.53. The root mean square error between the time series was 2.5 mm/yr. The PSI subsidence rates were on average 1.0 mm/yr slower than the rates measured in the FGI leveling. Even though the annual subsidence rates can be assumed constant for most of the buildings, it should be noted that there were temporal differences between the datasets, and it is likely that non-linearity exist in the subsidence rates of few buildings due to renovation works. Two benchmarks had very high subsidence rates of over 10 mm/yr measured in the FGI leveling, whereas the PSI results for the same buildings indicated subsidence of only about 5 mm/yr. Possible

causes for this are non-linear subsidence of the particular building or different objects being observed or the limits of PSI technique due to noise [41].

In addition, the FGI leveling observations along three leveling lines were compared to PSI observations (Figure 9). The trends are similar; however the rate of subsidence varies. Average absolute value of the difference was 1.6 mm/yr (Line1 1.8, Line2 0.9 and Line3 2.8 mm/yr). This is also likely caused by the observations referring to different buildings or other objects and they also cover different periods of time.

Figure 9. The FGI precise leveling results (annual subsidence rates) along three leveling lines and the PS observations along the lines. Note that the subsidence is not spatially continuous.

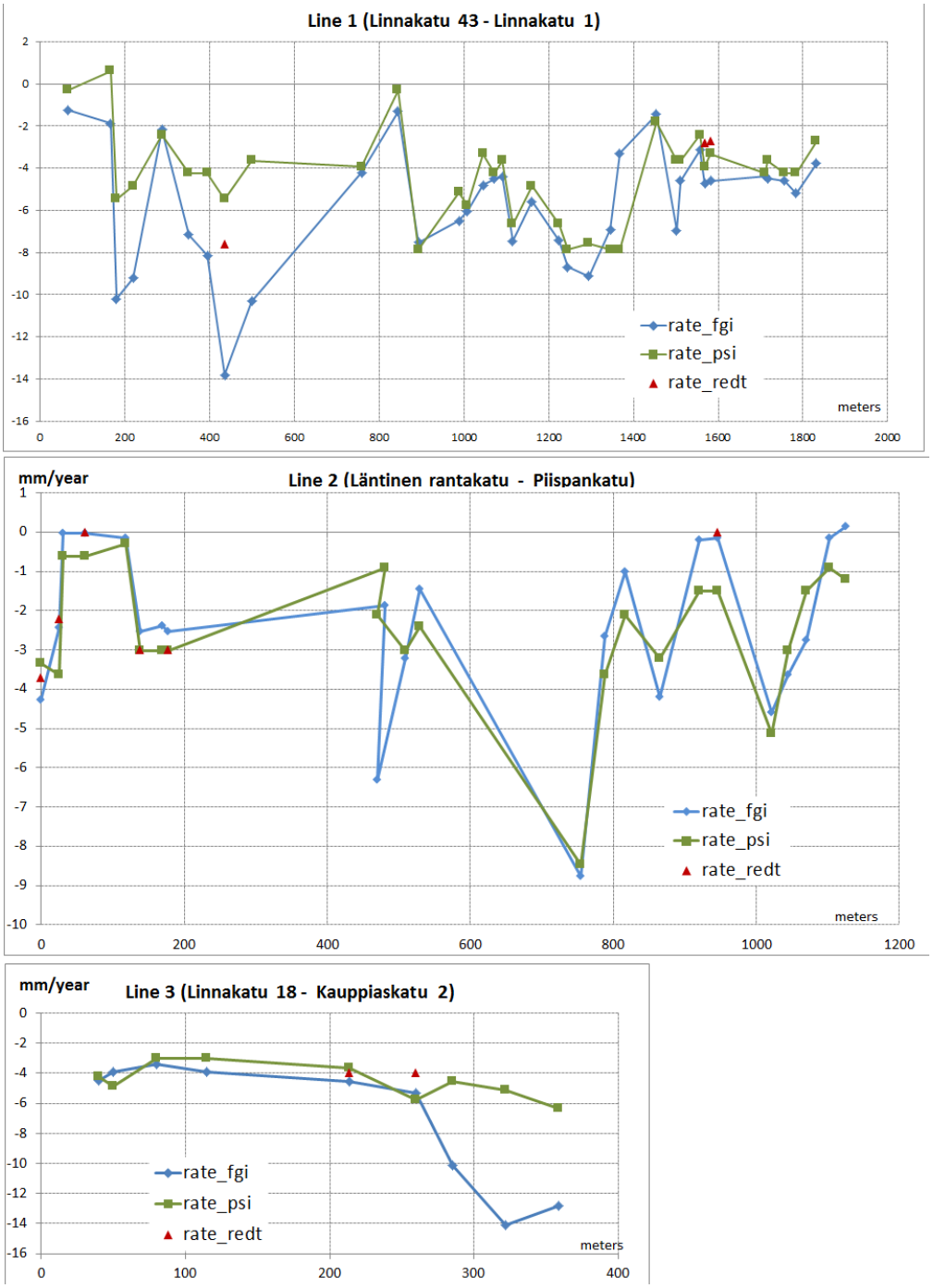

The TC values of the PSI observations were also studied. For the test set the accuracy of the CTM results in comparison to the leveling did not depend on the temporal coherence values. As indicated in Table 1 for lower TC values the deformation rates became noisy, however, this effect is not detectable in the data, which has the minimum TC of 0.6.

5. Discussion

The interpretation of the results is challenging because of the complexity of the geocoding and the uncertainty (5 m in azimuth and 20 m in range) concerning the source of scattering. A building plan or base map can be a useful aid in the refinement of coarse geocoding and can help to relate the PSI observations to the buildings. However, large SAR datasets and independent analyses are needed to ensure that precise locations are identified.

Temporal differences often exist between different datasets because it is difficult to obtain simultaneous data. Continuous SAR dataset is not always available due to satellite revisit times and acquisition priorities. For example, ERS and ENVISAT enabled data acquisition with the same geometry only once every 35 days. Modeling of non-linear deformation with irregularly acquired data is particularly difficult.

Historical SAR data are available, but ground truth data from the same period is usually difficult to find. Fortunately for this case study, a longer leveling time series was available for some of the buildings from the City's Real Estate Department. The FGI's leveling covers only a one-year period from 2005 to 2006. The FGI subsidence rates used in the analyses ranged from 0.15 to −14.1 mm/yr. In the PSI results (near the leveling sites), subsidence rates ranged from +5.5 to −9.7 mm/yr and the PSI values used in the analyses ranged from 0.6 to −8.5 mm/yr. In the PSI analysis, the entire SAR time series from 1992 to 2006 was used in order to ensure that there were enough images to obtain reliable results. Thus, there are large temporal differences in the datasets. Since the City's leveling data also indicated fairly constant subsidence rates for the benchmarks, the subsidence rate was assumed constant in order to compare the FGI's leveling and the PSI measurements. In the REDT long leveling time series, the deviation from linear subsidence was less than 1 mm, which was the same order of magnitude as the measurement error. However, it is likely that some buildings have discrepancies due to renovation works, *etc*., and so some errors are inevitable.

Using a satellite track we are able to extract only one component of the 3D deformation vector. Here, we expected that only vertical deformation is occurring. Thus any horizontal deformation will cause errors.

It should also be noted that some of the selected parameters and inputs have a considerable effect on the PSI analysis results. The reference area for the initial atmospheric phase estimation (the stable reference area) has to be selected carefully, since the error will be compounded in the results. The threshold used in the selection of the coherent targets also has a significant effect on the results, particularly the quality of the results. When lower temporal coherence values are used, the number of PSs increases and vice versa. Determination of the optimum value is not straightforward.

The analysis would benefit of the new high resolution SAR satellites (e.g., Terrasar-X, Cosmo-Skymed), which provide better estimate of the DEM error and more precise PS geocoding, denser PS sampling and higher quality of the PS time series [42]. Therefore, it is easier to relate a PS

to a part of a building. However, the exact source of scattering remains unknown. The high resolution would be also beneficial in determination of the reference area. Also, the sensitivity of the phase to deformation is higher in X-band due to shorter wavelength, and thus, smaller deformation can be detected. The shorter revisit times enable denser time series. Also, using high resolution X-band data, fewer SAR images are needed to get reliable displacement rates for the same time span [43].

6. Conclusion

In this study, we have carried out a comparison of non-continuous urban subsidence rates from spaceborne SAR interferometry and precise leveling of building foundations. Even though the comparison was affected by a number of problems, particularly spatial and temporal differences, the PSI results agreed rather well with the leveling data. R^2 value with the REDT data of 10 buildings was 0.96 and the mean deformation rate from PSI was on average 0.03 mm/yr slower than the mean deformation rate from leveling. R^2 value of PS and the FGI leveling of a nearby benchmark was 0.52. PS subsidence rates were on average 1 mm slower than the FGI leveling subsidence rates. According to the results, spatially discontinuous building subsidence occurring at a rate of a few mm/yr can be detected and this result was confirmed using the geodetic precise leveling data. Using PSI, a precision comparable to precise leveling is obtained over an urban area with a good spatial sampling. However, the parameters of the PSI analysis and the quality of output products should always be carefully considered when interpreting PSI results.

PSI of C-band medium resolution data is feasible in pinpointing problem areas in a built-up or otherwise stable environment and is a suitable technique for measuring building subsidence, since buildings usually act as persistent scatterers. The absolute accuracy of the technique depends on the datasets and parameters, and it cannot be determined without artificial reflectors with a known scattering source. In order to interpret the results and accurately measure the absolute subsidence rates, precise location of the persistent scatterers should be known and calibration targets for zero deformation (e.g., use of corner reflectors) should be used. Traditional surveying methods are still needed in areas where vegetation plays a major role (lack of persistent scatterers), in areas where long time series of satellite data is not available, subsidence is temporally complex, and subsidence rates are too high or too low to detect using PSI, for calibration of the relative PSI results and when accuracy in measuring building subsidence is paramount.

Acknowledgments

The authors would like to thank the anonymous reviewers for their valuable comments, which greatly improved the paper. The SAR images used in this study were provided by the European Space Agency (ESA) within the framework of Category-1 project 1422. The authors would also like to thank the City of Turku's Real Estate Department for providing the reference data**.** This work was supported in part by the Finnish Funding Agency for Technology and Innovation (Tekes).

Conflicts of Interest

The author declares no conflict of interest.

References

1. Precise Leveling: Contributions to the Workshop on Precise Levelling Held at the University of Hannover, 16–18 March 1983; Pelzer, H., Niemeier, W., Eds.; Ferd. Dümmlers Verlag: Bonn, Germany, 1984.
2. Ferretti, A.; Savio, G.; Barzaghi, R.; Borghi, A.; Musazzi, S.; Novali, F.; Prati, C.; Rocca, F. Submillimeter accuracy of InSAR time series: Experimental validation. *IEEE Trans. Geosci. Remote Sens.* **2007**, *45*, 1142–1153.
3. Ferretti, A.; Prati, C.; Rocca, F. Permanent scatterers in SAR interferometry. *IEEE Trans. Geosci. Remote Sens.* **2001**, *39*, 8–20.
4. Massonnet, D.; Feigl, K. Radar interferometry and its application to changes in the Earth's surface. *Rev. Geophys.* **1998**, *36*, 441–500.
5. Mora, O.; Mallorquí, J.J.; Broquetas, A. Linear and non-linear terrain deformation maps from a reduced set of interferometric SAR images. *IEEE Trans. Geosci. Remote Sens.* **2003**, *41*, 2243–2253.
6. Werner, C.; Wegmüller, U.; Strozzi, T.; Wiesmann, A. Interferometric Point Target Analysis for Deformation Mapping. In Proceedings of the IEEE Geoscience and Remote Sensing Symposium, IGARSS, Toulouse, France, 21–25 July 2003; pp. 4362–4364.
7. Kampes, B.; Adam, N. The STUN Algorithm for Persistent Scatterer Interferometry. In Proceedings of the Fringe 2005 Workshop, Frascati, Italy, 28 November–2 December 2005.
8. Hooper, A.; Zebker, H.; Segall, P.; Kampes, B. A new method for measuring deformation on volcanoes and other natural terrains using InSAR persistent scatterers. *Geophys. Res. Lett.* **2004**, *31*, doi: 10.1029/2004GL021737.
9. Van der Kooij, M.; Hughes, W.; Sato, S.; Poncos, V. Coherent Target Monitoring at High Spatial Density: Examples of Validation Results. In Proceedings of the Fringe 2005, Frascati, Italy, 1–5 December 2005.
10. Colesanti, C.; Ferretti, A.; Prati, C.; Perissin, D.; Rocca, F. ERS—Envisat Permanent Scatterers Interferometry. In Proceedings of the International Geoscience and Remote Sensing Symposium IGARSS 2003, Toulouse, France, 21–25 July 2003; Volume 2, pp. 1130–1132.
11. Duro, J.; Closa, J.; Biescas, E.; Crosetto, M.; Arnaud, A. High Resolution Differential SAR Interferometry Using Time Series of ERS and ENVISAT Data. In Proceedings of the FRINGE 2003 Workshop (ESA SP-550), Frascati, Italy, 1–5 December 2003.
12. Pepe, A.; Sansosti, E.; Berardino, E.; Lanari, R. On the generation of ERS/ENVISAT DInSAR time-series via the SBAS Technique. *IEEE Geosci. Remote Sens. Lett*. **2005**, *2*, 265–269.
13. Crosetto, M.; Biescas, E.; Duro, J.; Closa, J.; Arnaud, A. Generation of advanced ERS and ENVISAT interferometric SAR products using the stable point network technique. *Photog. Eng. Remote Sens*. **2008**, *74*, 443–450.
14. Raucoules, D.; Bourgine, B.; de Michele, M.; le Cozanet, G.; Closset, L.; Bremmer, C.; Veldkamp, T.D.; Bateson, L.; Crosetto, M.; Agudo, M. *Persistent Scatterers Interferometry Independent Validation and Intercomparison of Results*; Final Report, BRGM/RP-55649-FR; BRGM: Orléans, France, 2007.

15. Raucoules, D.; Bourgine, B.; de Michele, M.; le Cozanet, G.; Closset, L.; Bremmer, C.; Veldkamp, H.; Tragheim, D.; Bateson, L.; Crosetto, M.; *et al*. Validation and intercomparison of persistent scatterers interferometry: PSIC4 project results. *J. Appl. Geophys.* **2009**, *68*, 335–347.
16. Odijk, D.; Kenselaar, F.; Hanssen, R. Integration of Leveling and INSAR Data for Land Subsidence Monitoring. In Proceedings of the 11th FIG Symposium on Deformation Measurements, Santorini, Greece, 25–28 May 2003.
17. Heleno, S.; Oliveira, L.; Henriques, M.J.; Falcão, A.P.; Lima, J.N.; Cooksley, G.; Ferretti, A.; Fonseca, A.M.; Lobo-Ferreira, J.; Fonseca, J. Persistent scatterers interferometry detects and measures ground subsidence in Lisbon. *Remote Sens. Environ*. **2011**, *115*, 2152–2167.
18. Wegmüller, U.; Walter, D.; Spreckels, V.; Werner, C. Nonuniform ground motion monitoring with TerraSAR-X persistent scatterer interferometry. *IEEE Trans. Geosci. Remote Sens*. **2010**, *48*, 895–904.
19. Marinkovic, P.; Ketelaar, G.; Hanssen, R. A Controlled ENVISAT/ERS Persistent Scatterer Experiment, Implications of Corner Reflector Monitoring. In Proceedings of the CEOS SAR Workshop 2004, Ulm, Germany, 27–28 May 2004.
20. Savio, G.; Ferretti, A.; Novali, F.; Musazzi, S.; Prati, C.; Rocca, F. PSInSAR Validation by Means of a Blind Experiment Using Dihedral Reflectors. In Proceedings of the Fringe 2005 Workshop, Frascati, Italy, 28 November–2 December 2005.
21. Ketelaar, G.; Marinkovic, P.; Hanssen, R. Validation of Point Scatterer Phase Statistics in Multi-Pass INSAR. In Proceedings of the Envisat & ERS Symposium 2004, Salzburg, Austria, 6–10 September 2004.
22. Zhou, Y.; Stein, A.; Molenaar, M. Integrating interferometric SAR data with leveling measurements of land subsidence using geostatistics. *Int. J. Remote Sens.* **2003**, *24*, 3547–3564.
23. Karila, K.; Karjalainen, M.; Hyyppä, J. Urban land subsidence studies in Finland using synthetic aperture radar images and coherent targets. *Photogramm. J. Finl.* **2005**, *19*, 43–53.
24. Cascini, L.; Ferlisi, S.; Peduto, D.; Fornaro, G.; Manunta, M. Analysis of a subsidence phenomenon via DInSAR data and geotechnical criteria. *Ital. Geotech. J.* **2007**, *41*, 50–67.
25. Tomás, R.; García-Barba, J.; Cano, M.; Sanabria, M.P.; Ivorra, S.; Duro, J.; Herrera, G. Subsidence damage assessment of a gothic church using Differential Interferometry and field data. *Struct. Health Monit.* **2012**, *11*, 751–762.
26. Bru, G.; Herrera, G.; Tomás, R.; Duro, J.; de la Vega, R.; Mulas, J. Control of deformation of buildings affected by subsidence using persistent scatterer interferometry. *Struct. Infrastruct. Eng.* **2013**, *9*, 188–200.
27. Herrera, G.; Tomás, R.; Monells, D.; Centolanza, G.; Mallorqui, J.J.; Vicente, F.; Navarro, V.D.; Lopez-Sanchez, J.M.; Cano, M.; Mulas, J.; *et al*. Analysis of subsidence using TerraSAR-X data: Murcia case study. *Eng. Geol.* **2010**, *116*, 284–295.
28. Kahmen, H.; Faig, W. *Surveying*; Walter de Gruyter: Berlin, Germany, 1988.
29. Mäkinen, J.; Koivula, H.; Poutanen, M.; Saaranen, V. Vertical velocities in Finland from permanent GPS networks and from repeated precise levellings. *J. Geodyn.* **2003**, *35*, 443–456.
30. Hanssen, R. Satellite radar interferometry for deformation monitoring: A priori assessment of feasibility and accuracy. *Int. J. Appl. Earth Obs. Geoinf.* **2005**, *6*, 253–260.

31. Perissin, D.; Rocca, F. High accuracy urban DEM using permanent scatterers. *IEEE Trans. Geosci. Remote Sens.* **2006**, *44*, 3338–3347.
32. Tomas, R.; Romero, R.; Mulas, J.; Marturi, J.J.; Mallorqum, J.J.; Lopez-Sanchez, J.M.; Herrera, G.; Gutiirrez, F.; Gonzalez, P.J.; Fernandez, J.; *et al*. Radar interferometry techniques for the study of ground subsidence phenomena: A review of practical issues through cases in Spain. *Environ. Earth Sci.* **2013**, doi: 10.1007/s12665–013–2422-z.
33. Niemela, J.; Sten, C.G.; Taka, M.; Winterhalter, B. Summary: Quaternary Deposits in the Turku-Salo Map-Sheet Areas. In *Turun-Salon Seudun Maaperä*; Geological Survey of Finland: Espoo, Finland, 1987; pp. 78–80. Available online: http://arkisto.gtk.fi/mps/1043_2021.pdf (accessed on 19 June 2013).
34. Sentin, V. Turun Keskusta Vajoaa Yhä. *Turun Sanomat*, 16 September 1998.
35. Satoja Taloja Uhkaa Vajoaminen Turussa. *Tekniikka & Talous*, 24 April 2003.
36. Mei, S.; Poncos, V.; Froese, C. *Insar Mapping of Millimeterscale Ground Deformation over Frankslide, Turtle Mountain, Alberta*; ERCB/AGS Earth Sciences Report 2007–09; Alberta Energy Resources Conservation Board and Alberta Geological Survey: Edmonton, Alberta, Canada, 2008.
37. *EV-InSAR User's Guide, Version 3.1*; Atlantis Scientific Inc.: Ottawa, ON, Canada, 2004.
38. *Local X-Positioning System. User's Manual*; X-Position Ltd.: Espoo, Finland, 1998.
39. Karila, K.; Karjalainen, M.; Hyyppä, J.; Saaranen, V. Test Field for INSAR Urban Subsidence Studies. In Proceedings of the Envisat Symposium 2007, Montreux, Switzerland, 23–27 April 2007.
40. Agudo, M.; Crosetto, M.; Raucoules, D.; Bourgine, B.; Closset, L.; Bremmer, C.; Veldkamp, H.; Tragheim, D.; Bateson, L. *PSIC4—Defining the Methods for PSI Validation and Intercomparison*; BRGM/RP-55636-FR; BRGM: Orléans, France, 2006.
41. Raucoules, D.; Colesanti, C.; Carnec, C. Use of SAR interferometry for detecting and assessing ground subsidence. *C. R. Geosci.* **2007**, *339*, 289–302.
42. Crosetto, M.; Monserrat, O.; Iglesias, R.; Crippa, B. Persistent scatterer interferometry: Potential, limits and initial C- and X-band comparison. *Photog. Eng. Remote Sens.* **2010**, *76*, 1061–1069.
43. Bovenga, F.; Wasowski, J.; Nitti, D.O.; Nutricato, R.; Chiaradia, M.T. Using COSMO/SkyMed X-band and ENVISAT C-band SAR interferometry for landslide analysis. *Remote Sens. Environ.* **2012**, *119*, 272–285.